Scaling of Vorticity Flux and Entrance Length Effects in Zero-Net Mass-Flux Devices

Reni Raju* and Rajat Mittal†
Department of Mechanical and Aerospace Engineering
The George Washington University, Washington, DC- 20052

Quentin Gallas* and Louis Cattafesta‡
Department of Mechanical and Aerospace Engineering
University of Florida, Gainesville, FL- 32611

Two-dimensional numerical simulations are used to examine the vorticity flux and slot entrance effects in zero-net mass-flux devices. The simulations allow us to extract a simple scaling law for the vorticity flux which provides insight into the relative importance of the various operational parameters. In addition to this, a semi-analytical model is proposed in order to determine the pressure loss across an orifice or slot for oscillatory flows. A key parameter in this model is the normalized entrance length and numerical simulations are used to determine the variation of this parameter with the jet Strouhal number.

Nomenclature

d = slot width, m
D = cavity depth, m
δ = boundary layer thickness, m
h = slot height, m
h_c = channel height, m
H = cavity height, m
ξ_z = z-component of vorticity, s^{-1}
L_E = entrance length, m
υ = kinematic viscosity, m^2/s
Ω_v = flux of vorticity, m^2/s
ω = radian frequency, Hz
p = pressure, N/m^2
ϕ = phase angle, degrees
Q = volumetric flow rate, m^2/s
Re = Reynolds number, $\mathrm{Re}_j = \overline{V}_j d/\upsilon$, $\mathrm{Re} = \overline{u} d/\upsilon$
St = Strouhal number, $St = \omega d/\overline{V}_j$, $St = \omega d/\overline{u}$
S = Stokes number, $S = \sqrt{\omega d^2/\upsilon}$, $S = \sqrt{\omega h_c^2/\upsilon}$
T = Forcing period, $T = 2\pi/\omega$
u = x-component of velocity , m/s
$\overline{u}$ = averaged velocity, m/s
U_o = Velocity amplitude, m/s
U_∞ = Cross-stream velocity , m/s
v = y-component of velocity, m/s
$\overline{V}_j$ = averaged jet velocity, m/s
W = width of cavity, m

Subscripts
i = indicial notations

I. Introduction

Zero-net mass-flux (ZNMF) devices, or synthetic jets as they are popularly known, have proven to be versatile devices. The versatility of these devices is primarily because they provide unsteady forcing, which is more effective than its steady counterpart, and since the jets are synthesized from the working fluid itself complex fluid circuits are not required. Moreover, actuation frequency and waveform for these devices can usually be adjusted to a particular flow configuration.

A typical synthetic jet actuator consists of a jet orifice opposed on one side by an enclosed cavity consisting of three components: an oscillatory driver, a cavity, and an orifice or slot as shown in Fig. 1. The oscillating driver compresses and expands the fluid in the cavity by changing the cavity volume at an excitation frequency to create

* Graduate Student, Student Member AIAA.
† Associate Professor, Senior Member AIAA.
‡ Associate Professor, Associate Fellow AIAA.

pressure oscillations. Due to time-periodic changes in the cavity volume a jet is synthesized from the entrained fluid, and if these changes are sufficiently strong, a train of vortex rings are generated at the edge of the orifice. Thus even with a zero net mass-flux through the orifice, the actuator imparts a finite momentum to the surrounding fluid. Interaction of the jet with an external flow can lead to closed recirculation regions which, in turn, lead to significant global effects on the flow boundary, like modification of the pressure distribution, on scales larger than the characteristic length scales of the synthetic jets themselves[1,2].

Extensive experimental and numerical investigations have been carried out for synthetic jets operating both in a quiescent medium and interacting with an external boundary layer in the aforementioned applications. Glezer and Amitay[3] have provided a comprehensive review on the evolution of synthetic jets and related work. Most of these studies have found that the performance characteristics of ZNMF devices are governed by a number of geometrical, structural and flow parameters[4-8]. However, there is still insufficient understanding as to how the performance of these devices scales with the governing parameters. Utturkar et al.[9] have carried out studies for parametric characterization of jets in a quiescent medium. The authors proposed and validated a jet formation criterion as a function of the ratio of jet Reynolds number to Stokes number for sharp orifices. Similar jet formation criterion based on the non-dimensional stroke length have been presented recently by Milavonic and Zaman[10]. Shuster and Smith[11] have concluded that both the orifice geometry and the non-dimensional stroke length determine whether a synthetic or a pulsed jet is formed. For a synthetic jet in a crossflow, however, the important issue is that of penetration of the boundary layer. For transverse jets in crossflow, studies indicate that the maximum jet penetration for improved mixing occurs for specific values of jet Strouhal numbers[12,13]; however similar parametric investigations are lacking for synthetic jets in crossflow. A parameter considered key to characterizing the jet is the momentum coefficient C_μ [14,15], generally defined as the ratio of the momentum imparted by the jet to the momentum of the external flow. A recent study shows that the penetration height for a synthetic jet in a crossflow increases with the increasing stroke length for a fixed frequency and crossflow velocity[10].

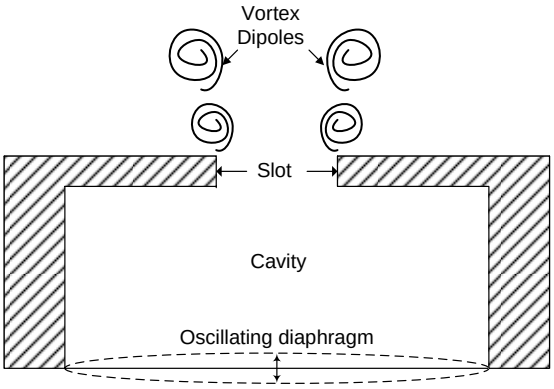

Figure 1. A typical sharp lipped synthetic jet in a quiescent medium.

The purpose of the current study is to develop a better understanding of the influence of these parameters on the flow characteristics of ZNMF actuators. This study focuses on two separate aspects of ZNMF devices: (1) the local interaction between a synthetic jet and incoming boundary layer in order to develop a scaling law for vorticity flux and (2) a semi-analytic model for calculating a loss coefficient in oscillatory slot/orifice flows at low Reynolds numbers. Similar to the scaling presented by Utturkar et al.[9], the importance of the functional dependence of the vorticity flux on key operational parameters is investigated. The focus here is on extracting a scaling law which relates the vorticity flux to both the Strouhal number and the ratio of external velocity to jet velocity. It is expected that the scaling laws developed from the current study will form an essential component in the design and deployment of ZNMF actuators in practical applications.

Furthermore, the development of low-dimensional models of synthetic jet requires a better understanding of the pressure losses across the orifice height. These are difficult to measure experimentally and numerical simulations provide a viable alternative. Depending on the flow parameters, the pressure losses might be linear and/or non-linear[16]. In the current paper, we propose a semi-theoretical model based on the full Navier-Stokes (N-S) equations and use simulations to evaluate the scaling of unknown coefficients in this model.

II. Scaling Arguments

A. Vorticity Flux Scaling for ZNMF actuators

The entrainment and expulsion of fluid by the actuator can lead to the formation of vortices that promote mixing and even transition of a laminar boundary layer. The expelled vortices transfer momentum to the external boundary layer and also lead to time-averaged recirculation bubbles in the proximity of the slot which might be suitable for certain applications[17]. Hence in addition to the momentum coefficient, characterization of the vorticity flux during the expulsion phase is also important[18]. Past simulations and experiments have shown that the vorticity flux during

expulsion determines whether a synthetic jet is formed in quiescent flow[9]. This time-averaged flux of vorticity, Ω_v across a planar slice during the expulsion phase can be defined as,

$$\Omega_v = \int_0^{T/2} \int_0^d \xi_z v dx dt \tag{1}$$

where v is the axial jet velocity component. Simple scaling arguments led to the conclusion that the non-dimensional vorticity flux is inversely proportional to the Strouhal number, and jet formation requires that the vorticity flux is larger than a critical value[9]. Thus the formation criterion is $\frac{\Omega_v}{\overline{V}_j d} \sim St^{-1} > K$, where the constant K is 2.0 and 0.16 for two-dimensional and axisymmetric jets, respectively[9]. In the presence of crossflow, additional parameters such as δ / d and $U_\infty / \overline{V}_j$, are also expected to influence the vorticity flux. In general, for jets in crossflow, the following minimum functional dependence is expected

$$\frac{\Omega_v}{\overline{V}_j d} = fn\left(\mathrm{St}, \frac{U_\infty}{\overline{V}_j}, \frac{\delta}{d}, \mathrm{Re}_j \right) \tag{2}$$

In the current paper, we use numerical simulations and experiments to extract the above scaling law for the case of zero pressure-gradient laminar boundary layer.

B. Entrance Length Effects

The ratio of pressure drop to volume flow rate, $\Delta p / Q$, called acoustic impedance, is an important parameter in low-order models of synthetic jets. For ZNMF devices, since the jet slot is relatively short, it is expected that entrance and end-effects will contribute significantly to the pressure losses. Determination of these entrance and end-effects is best accomplished through numerical simulations.

Unsteady pipe and channel flows, both oscillatory and pulsatile, have been investigated due mostly to their applications in biological systems. By definition, oscillatory flows have a zero time-averaged velocity where the velocity is generally given as $u = U_o \sin(\omega t)$; pulsatile flows are usually prescribed by $u = U_o + \sin(\omega t)$ and therefore have a non-zero time-averaged velocity. Although several researchers have extensively investigated entrance effects in steady flows[19-23] and pulsatile flows[24,25], only a few have documented these effects for purely oscillatory flows.[26,27] In the current study we develop a semi-analytical model for predicting the entrance losses and use numerical simulations to provide empirical data for the closure of the semi-analytic model.

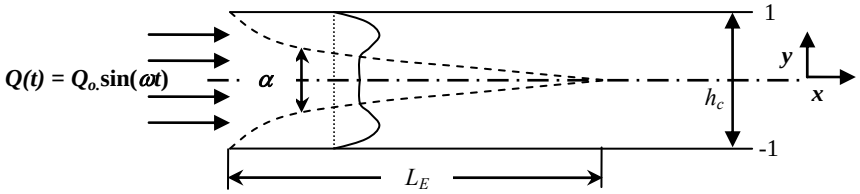

Figure 2. Schematic of entrance flow in a channel.

The governing equations for flow through 2-D channel of height h_c = 2 with rigid walls, depicted in Fig. 2, can be non-dimensionalized based on the definition of the Stokes number, S . Using the BL assumptions and integrating across of the height of the channel, the governing equation can be expressed in terms of the axial velocity u as

$$S^2 \frac{\partial Q}{\partial t} + \frac{\partial}{\partial x} \int_{-1}^{1} u^2 dy = -2 \frac{\partial \overline{p}}{\partial x} + 2 \left. \frac{\partial u}{\partial y} \right|_1 \tag{3}$$

where $Q(t)$ and $\overline{p}$ are the volumetric flow rate and spatial-averaged pressure across the channel height, respectively. We then assume an axial velocity profile of the following form based on the analytical solution for developing steady laminar flow in a channel given by Fargie and Martin[21],

$$u = \begin{cases} u_o(t) & \text{for } 0 \le y \le \alpha(x) \\ u_o(t) f(\alpha, y, S) & \text{for } \alpha(x) \le y \le 1 \end{cases} \tag{4}$$

where $f(\alpha, y, S) = \text{Real}\left[\frac{\cosh(S') - \cosh(S'z)}{\cosh(S') - 1}\right]$ is based on the theoretical model given for oscillatory, fully-developed, pressure-driven channel flow by Loundon and Tordesillas[28]. Here $u_o(t)$ is the oscillatory velocity in the jet core, $\alpha(x)$ is the core height, (1-α) is the boundary layer thickness, $S' = S\sqrt{i}$ and $z = \frac{y-\alpha}{1-\alpha}$. It should be pointed out here that there is an implicit assumption in Eq. (4) that the velocity is in phase at each time instant across the entire development length. This might not necessarily be the case, and this assumption requires further evaluation.

The continuity equation yields the form of $u_o(t)$

$$u_o(t) = \frac{Q(t)}{2(\alpha + (1-\alpha)K_1(S))} \tag{5}$$

where $K_1(S) = \frac{1}{\cosh(S') - 1}\left[\cosh(S') - \frac{\sinh(S')}{S'}\right]$ is a known function of S. Integration of the momentum equation along the channel length then yields the following form for the pressure loss,

$$\overline{p}_{L_E} - \overline{p}_0 = -\frac{S^2}{2}\frac{\partial Q}{\partial t}L_E - \frac{Q^2}{4}\left[\frac{K_2(S)}{\left(K_1(S)\right)^2} - 1\right] - \frac{QK_3(S')}{2}\int_0^{L_E}\frac{dx}{(1-\alpha)\left(\alpha + (1-\alpha)K_1(S)\right)} \tag{6}$$

where $K_2(S) = \int_0^1 f(\alpha, y, S)^2 dz$ and $K_3(S) = \frac{S'\sinh(S'z)}{\cosh(S') - 1}$ are again known integral functions of S, and L_E is the unknown entrance length. This expression can further be modified to give the loss coefficient across the entrance region of the channel as,

$$K_E = 2\left(\overline{p}_{L_E} - \overline{p}_0\right) = \underbrace{-S^2\frac{\partial Q}{\partial t}L_E}_{I} \underbrace{- \frac{Q^2}{2}\left[\frac{K_2(S)}{\left(K_1(S)\right)^2} - 1\right]}_{II} \underbrace{- QK_3(S')\int_0^{L_E}\frac{dx}{(1-\alpha)\left(\alpha + (1-\alpha)K_1(S)\right)}}_{III} \tag{7}$$

Term *I* on the RHS represents the loss coefficient due to the inviscid acceleration, *II* is due to *entrance loss* from the nonlinear convective term, and term *III* is due to viscous effects. Hence we can obtain a closed form expression to determine the loss coefficient in the entrance length of a channel if $\alpha(x)$ and L_E are known. In fact, one can assume a simple form for $\alpha(x)$, but L_E still needs to be determined as a function of other parameters. It is known from previous work that the entrance length for pulsatile flows scales as $L_E/h = 2.64/St$.[29] The objective here is to develop a similar scaling law for the entrance length as a function of Strouhal number and Stokes (or Reynolds) number for a purely oscillatory flow using numerical simulations. This then can be used to obtain an expression for $\alpha(x)$, yielding finally a complete solution for the loss coefficient.

III. Simulation Overview

A. Numerical Methodology

A synthetic jet issuing from a cavity is modeled by the unsteady, incompressible Navier-Stokes equations, written in tensor form, as

$$\begin{aligned} &\frac{\partial u_i}{\partial x_i} = 0 \\ &\frac{\partial u_i}{\partial t} + \frac{\partial (u_i u_j)}{\partial x_j} = -\frac{\partial p}{\partial x_i} + \frac{1}{\text{Re}}\frac{\partial^2 u_i}{\partial x_j \partial x_j} \end{aligned} \tag{8}$$

where the indices, i = 1, 2, 3 represent the $x_1(x), x_2(y), x_3(z)$ directions, respectively, p is the pressure and the components of the velocity vector u_i are denoted by $u_1(u)$, $u_2(v)$ and $u_3(w)$ respectively. The equations are non-dimensionalized with the appropriate length and velocity scales, and Re is the Reynolds number. The Navier-Stokes equations are discretized using a cell-centered, collocated (non-staggered) arrangement of the primitive variables

velocity, u_i and pressure, p. In addition to the cell-center velocities (u_i), the face-center velocities (U_i), are also computed. Similar to a fully staggered arrangement, only the component normal to the cell-face is calculated and stored. The face-center velocity is used for computing the volume flux from each cell. The advantage of separately computing the face-center velocities has been initially proposed by Zang et al.[30] and discussed in the context of the current method in Ye at al.[31] The equations are integrated in time using a second-order accurate fractional step method. In the first step, the pressure field is computed by solving a Poisson equation. A second-order Adams-Bashforth scheme is employed for the convective terms while the diffusion terms are discretized using an implicit Crank-Nicolson scheme which eliminates the viscous stability constraint. The pressure Poisson equation is solved with a Krylov-based approach. A multi-dimensional ghost-cell methodology is used to incorporate the effect of the immersed boundary on the flow. The general framework can be considered as Eulerian-Lagrangian, wherein the immersed boundaries are explicitly tracked as surfaces in a Lagrangian mode, while the flow computations are performed on a fixed Eulerian mesh. Care has been taken to ensure that the discretized equations satisfy local and global mass conservation constraints as well as pressure-velocity compatibility relations. The code has been rigorously validated by comparisons of several test cases against established experimental and computational data[32,33].

B. Flow Configuration for Synthetic Jet simulations

To simulate a synthetic jet at the slot exit, the numerical simulations impose an oscillatory boundary condition $U_o\sin(\omega t)$ at the bottom of the cavity. Figure 3(a) shows the implementation of the boundary conditions for a typical 2D synthetic jet in a crossflow. For a jet in a quiescent external flow, the three governing parameters are the jet Reynolds number Re_j, Stokes number S and h/d ratio. The Strouhal number (St) can also be used in place of either the Reynolds number or the Stokes number. The effectiveness of the synthetic jet to impart momentum to its surroundings is highly dependent on these parameters and the slot/orifice geometry. The presence of a crossflow brings in at least two additional parameters; $U_\infty / \overline{V}_j$ and δ / d. A typical 2-D grid for a rectangular synthetic jet in a crossflow in the vicinity of the jet exit is shown in Fig. 3(b).

Since the number of parameters to be examined is large, we have restricted the analysis to low jet Reynolds number cases with a laminar boundary layer in crossflow. In addition, the geometry and the ratio δ / d is held fixed for all runs, while Re_j and S are varied to obtain different values of St. In another instance, St is held fixed while the ratio $U_\infty / \overline{V}_J$ is varied. The details of the computations have been listed in Table 1.

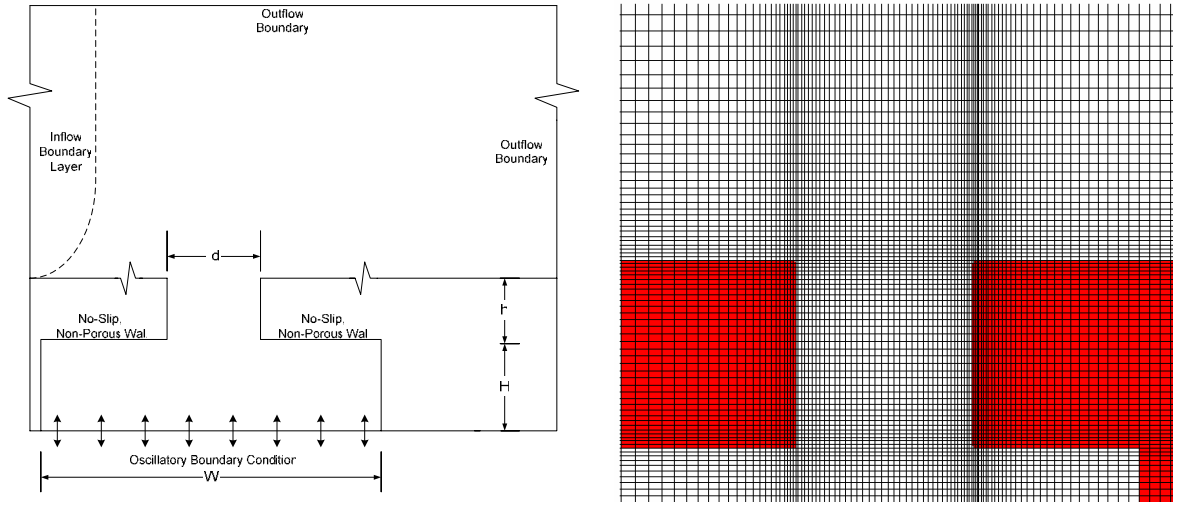

(a) (b)

Figure 3. (a) Synthetic jet computational boundary conditions and (b) a typical Cartesian grid in the vicinity of the slot.

Table 1. Computational details and range of parameters used for the vorticity flux simulations.

Domain $(L_x \times L_y)$	Grids $(N_x \times N_y)$	Dimensions held Constant	Range of Re_j	Range of S	Range of $U_\infty / \overline{V}_j$
$10d$x$10d$	154×127 198×177	h/d = 1.0 δ/d = 2.0 W/D = 3.0 H/D = 1.5	93.75 125 250 500	5 10 20 50	0.5 1.0 2.0 3.0 4.0

C. Flow Configuration for Entrance Flow simulations

Two types of entrance configurations have been studied. Figure 2 shows a straight channel with an oscillatory velocity profile prescribed at the inlet. Such a channel represents the model configuration of a jet with a smooth entrance. In addition, a channel with sharp-corners at the entrance is also chosen, as seen in Fig. 4. A similar configuration has been used to study entrance losses for steady flow calculations[34].

The details of the channel dimensions based on the channel height h_c and grids used are listed in Table 2. For both cases the inlet conditions are specified similar to a synthetic jet, where an oscillatory plug velocity profile $U_o\sin(\omega t)$ is prescribed. For the sharp orifice the inlet domain is of size $5h_c$ x $2h_c$ where h_c is the channel height. In both cases the Reynolds number is based on averaged velocity during the expulsion stroke.

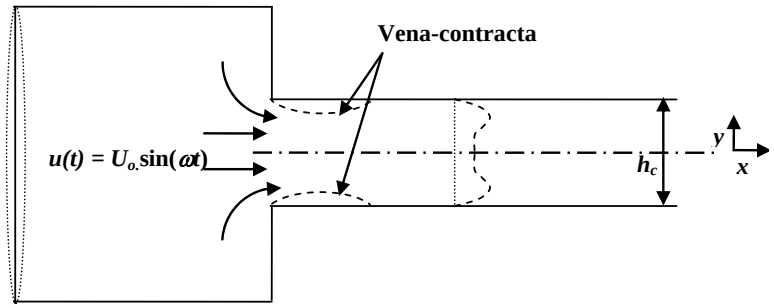

Figure 4. Schematic of entrance flow in a channel with a sharp-corner.

Table 2. Computational details and range of parameters used for the entrance effect simulations.

Channel Dimensions $(L_x \times L_y)$	Grids $(N_x \times N_y)$	Range of Re	Range of S
$1h_c \times 20h_c$ $1h_c \times 30h_c$	54×251 107×1001	50 100 250 500 1000	5 10 15 20 30 31.7
$5h_c \times 2h_c + 1h_c \times 50h_c$	81×685		

IV. Results

A. Vorticity Flux Scaling

Figure 5 shows experimental data (for a circular orifice) on non-dimensional vorticity flux as a function of St in a quiescent external flow for varying S from 4 to 53.6. Details of these experiments are described in Gallas[35]. Use of the log scale shows that over the range of St (0.068 – 25.4), the vorticity flux exhibits a power-law trend that seems to vary linearly with S. This is consistent with the simple scaling law of Utturkar et al.[9] The objective in the current study is to determine if a jet in crossflow exhibits a similar scaling law.

For simulations with crossflow the Reynolds number based on the boundary layer thickness $\left(\mathrm{Re}_\delta = U_\infty \delta / \upsilon\right)$ is varied from 125 to 4000, while St is varied between 0.1 – 26.7. Figure 6 shows the vorticity contours of a synthetic jet interacting with a laminar boundary layer at Re_δ=1000 for St = 0.8 and 20.0. For St = 0.80 (Re_j = 125, S = 10) the expelled vortices are swept away by the laminar boundary layer. For the same Re_j = 125 at significantly higher Strouhal number, the vortices formed are not completely expelled but are reingested. This indicates that for very high St, the vorticity flux might not have a significant effect on the boundary layer.

The normalized instantaneous vorticity flux, based on the magnitude of the vorticity across the slot exit, is shown in Fig. 7 as a function of phase angle. The plot shows a periodic behavior indicating that the flow has reached a stationary state. The magnitude of the vorticity is calculated by time-averaging over the expulsion half of the cycle.

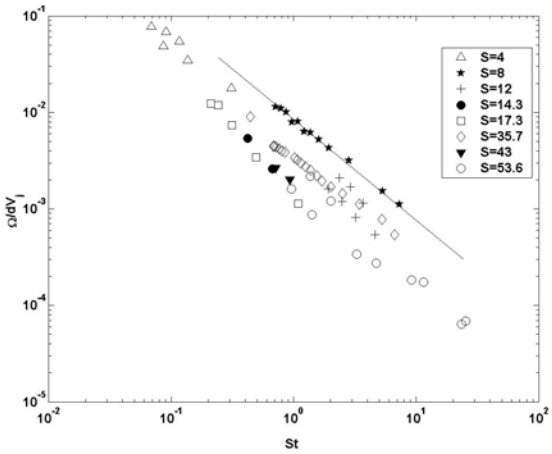

Figure 5. Experimental results for vorticity flux as a function of Strouhal number for different Stokes numbers.

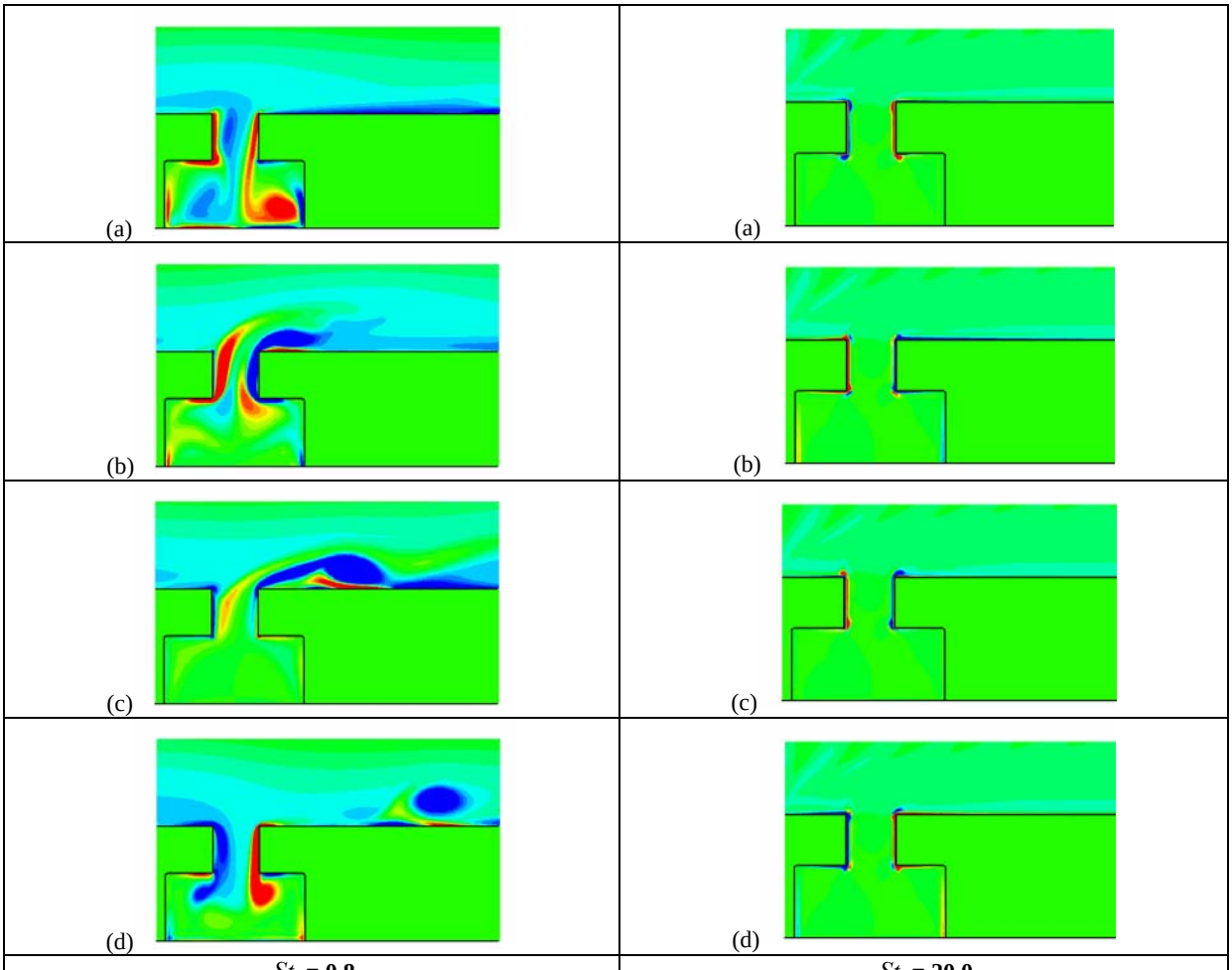

St = 0.8	St = 20.0

Figure 6: Comparison of the vorticity contours for St = 0.8 and St = 20.0 at phase angles, (a) ϕ = 0°, (b) ϕ = 90°, (c) ϕ = 180° and (d) ϕ = 270° of a cycle. Note that ϕ = 0° is the start of the expulsion stroke.

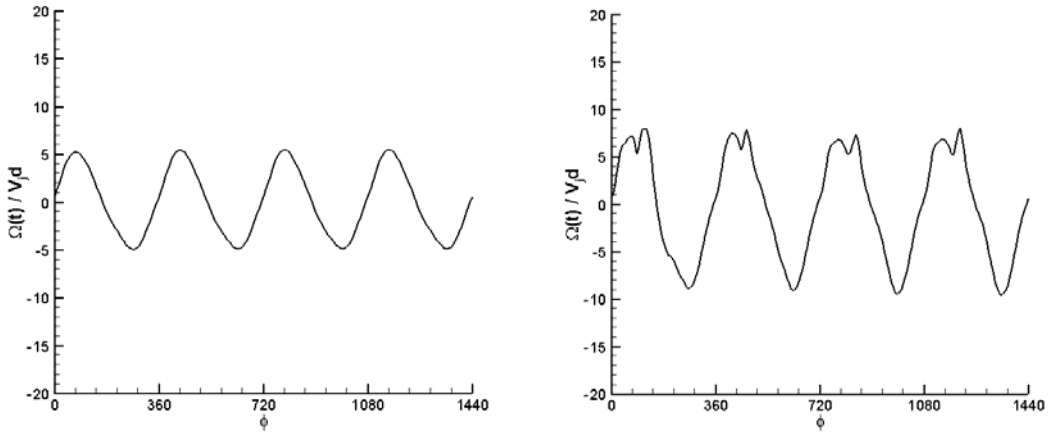

(a) (b)

Figure 7: Normalized $\Omega_v(t)$ across the slot exit as a function of the phase for four cycles, (a) St = 3.2 and $U_\infty / \overline{V}_j$ = 4, (b) St = 1.6 and $U_\infty / \overline{V}_j$ = 2.

While fixing $U_\infty / \overline{V}_j$ = 4, S is varied for a particular Re_j, which yields four data sets with different Re_j. A comparison of the time-averaged vorticity flux versue the St reveals a negative power-law type behavior at all Reynolds numbers, as seen in Fig. 8(a). This is similar to the experimental findings for quiescent flows shown previously in Fig. 5. The vorticity flux also reveals an approximately linear dependence on $U_\infty / \overline{V}_J$ over a range of 0.5 to 4 at a fixed Re_j and St, as seen in Fig. 8(b). This indicates that the non-dimensional vorticity flux can be expressed as a combination of these two parameters

$$\frac{\Omega_v}{\overline{V}_J d} = \alpha(\mathrm{Re}_j)\, St^{-\beta}\left(\lambda + \frac{U_\infty}{\overline{V}_j}\right) \tag{9}$$

where α is an unknown function of Re_j, and β and λ are constants that also need to be determined. Nonlinear regression analysis of the available data yields the values of the four constants listed in Table 3. We have found that among many possible functional dependencies on Re_j, a simple log-law provides acceptable accuracy.

Table 3. Constants obtained for the scaling law.

Constant	Value
λ	3.9
β	0.9
$\alpha(\mathrm{Re}_j)$	$0.66 \times \ln\left(\frac{\mathrm{Re}_j}{4.04}\right)$

Hence we find a scaling law for the vorticity flux that varies with the natural logarithm of Re_j, a negative power of St, and a linear function of $U_\infty / \overline{V}_j$. Equation (9) is plotted in Fig. 8 along with the computed data, and we see that the fit is reasonable for most cases.

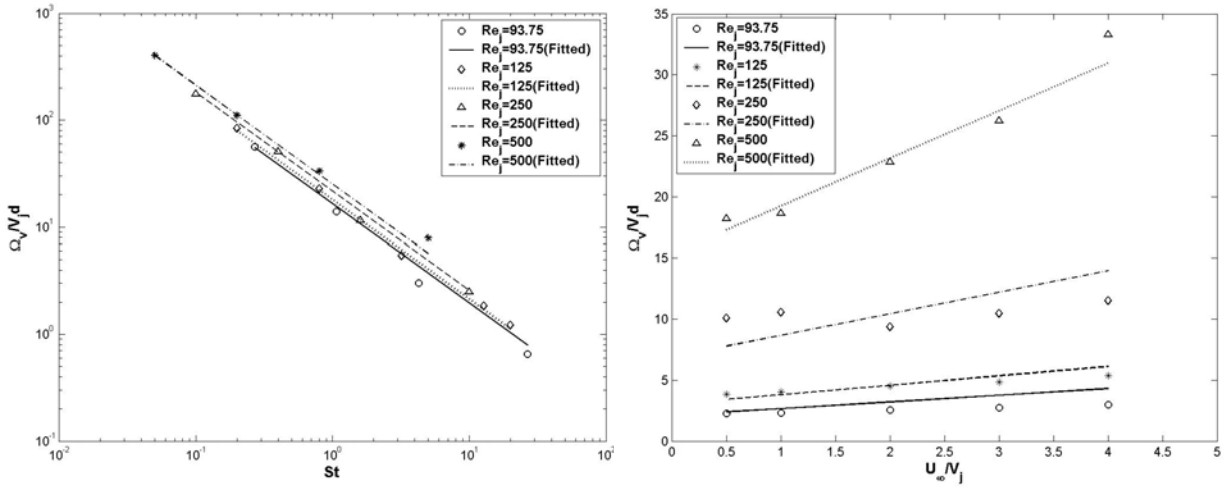

(a) (b)

Figure 8: Vorticity flux as a function of (a) Strouhal number and (b) $U_\infty / \overline{V_J}$ at different Re_j.

B. Entrance Length Scaling

Simulations were carried out to determine the entrance length for low Reynolds numbers ranging from 50 to 1000 and Stokes number from 5 to 50, since most ZNMF devices operate in this range. Grid independence studies showed that the variation in results is less than 0.4 %. The first set of simulations was carried out for a straight channel corresponding to an orifice with a rounded edge for the expulsion cycle only. The entrance length was calculated based on the length in the streamwise direction where the velocity reaches 99% of its peak value. Figure 9 show the entrance length as a function of phase angle for Re = 50, 100, 250 and 500, respectively, at different Stokes numbers. For higher values of Stokes number the flow tends to have lower entrance lengths due to a decrease in the time required for the flow to develop, whereas the flow tends to reach a quasi-steady state for lower values of Stokes number. Also note that higher Reynolds number flows require longer entrance lengths. These results clearly show that the entrance length L_E is a function of both Re and S. Since the simulations were restricted to the first half cycle (i.e., the expulsion stroke 0º–180º), we do not see the phase difference for the entrance lengths with increasing Stokes number that has been observed in the case of pulsatile flows[25].

Instead of using the maximum entrance length values we instead calculated the average entrance length values over the half cycle. Figure 10(a) plots the normalized average entrance length as a function of S for five different Re ranging from 50 to 1000. It shows a rapid exponential decay for higher S converging to an asymptotic value of L_E. A similar observation was made for pulsatile flows with varying Womersley number ($R\sqrt{\omega/\upsilon}$, R being the radius of a tube) based on the maximum entrance length[25]. On the other hand, the variation of the entrance length versus the Reynolds number reflects a linear behavior, which is seen in Fig. 10(b). These results indicate that for sufficiently high values of S, the entrance length becomes independent of the Reynolds number, as is seen for S = 30. This implies that while jet frequency is important, viscous effects are relatively unimportant and suggests that an inviscid frequency parameter such as St may be appropriate for scaling. The variation of the average entrance length versus St for the different Re is shown in Fig. 11. In general, the various curves collapse, particularly for St greater than ~1. Even for lower values of St, the entrance length shows a power-law trend, which suggests that it can be scaled directly with the inverse power of St. This corresponds to observations made earlier for pulsatile flows.[29]

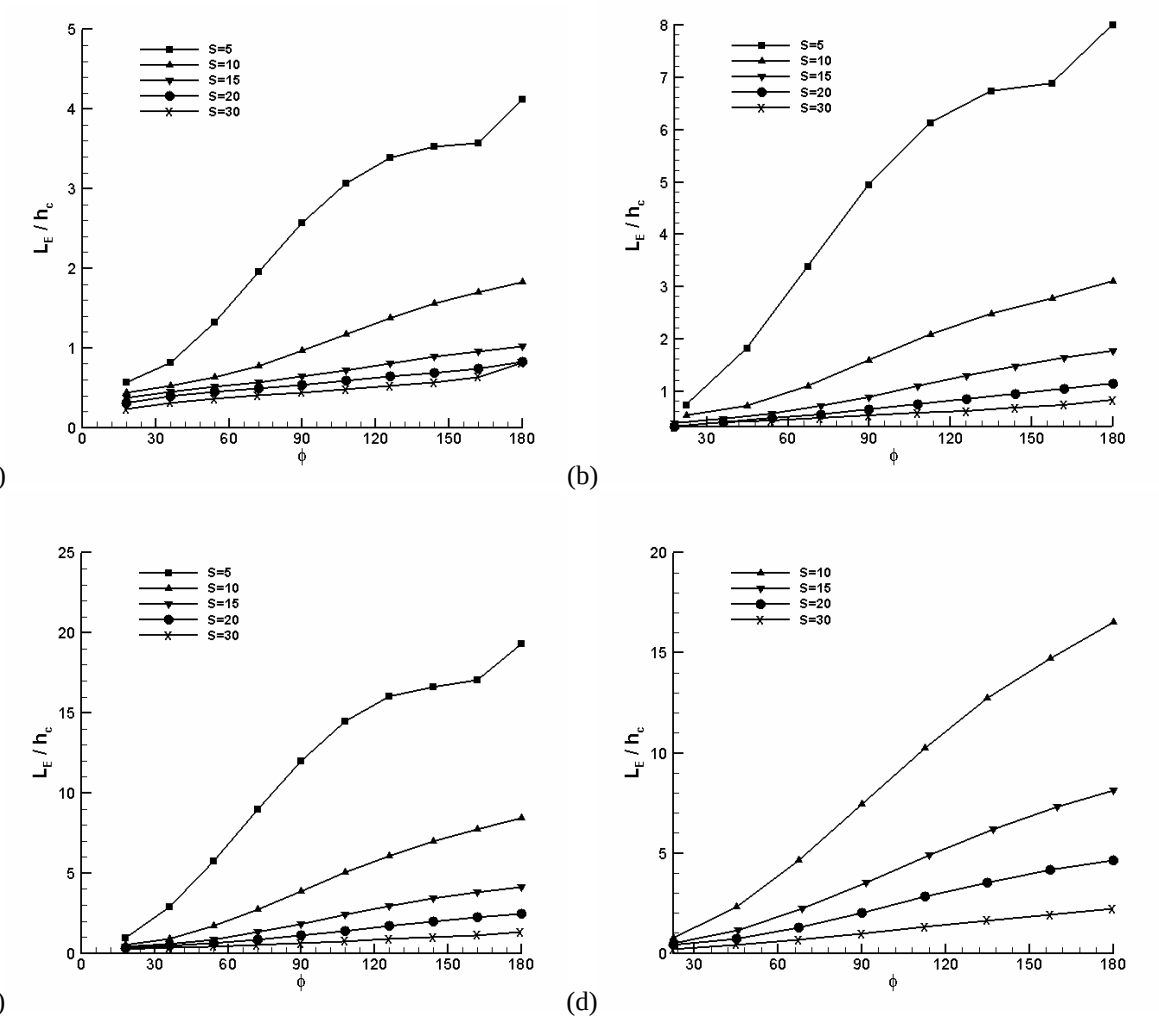

Figure 9: Entrance length variation as a function of phase for varying Stokes number at (a) Re = 50, (b) Re = 100, (c) Re = 250 and (d) Re =500.

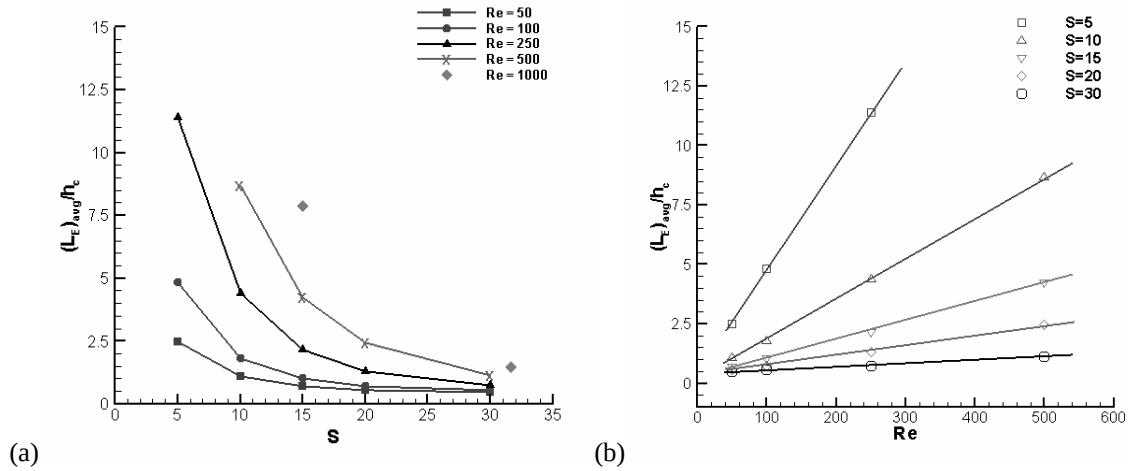

Figure 10: Average entrance length as a function of (a) Stokes number, and (b) Reynolds number.

From the point of view of ZNMF actuators used in practical applications, the flow configuration of a channel with a sharp entrance is more relevant. The simulations were repeated for the same set of parameters as that of the purely straight channel, and it was observed that both flows are inherently different. Due to the sharp corner, the flow in the inlet region of the channel develops a vena-contracta during the expulsion cycle, as illustrated in Fig. 4. The size of vena-contracta varies during the cycle and disappears during the ingestion phase where a counter-rotating pair of vortices is formed near the lip of the entrance. Thus the flow is significantly more complicated in this second case.

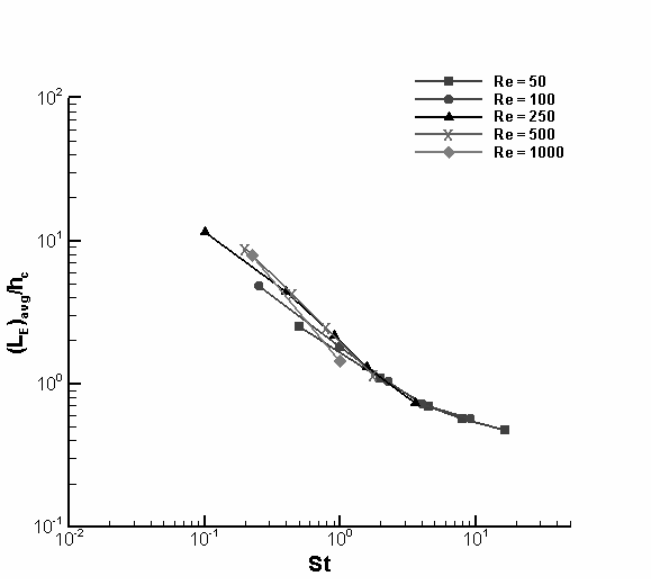

Figure 11: Average entrance length as a function of Strouhal number.

Figure 12 shows the velocity profiles at the entrance for the second flow configuration for two different Stokes numbers. For the lower Stokes number case, during the expulsion stroke the velocity magnitude near the center is slightly less than the near wall values, which is characteristic of oscillatory flows. However during the peak ingestion stroke the flow profile is found to be completely parabolic as seen in Fig. 12(a), which is inherently different from the peak expulsion stroke profile. For the higher Stokes number case, seen in Fig. 12(b), the velocity profiles exhibit the "Womersley" type profile, found in fully-developed oscillatory flows, at all phases in the cycle.

As mentioned earlier there are some inherent difficulties associated with the determination of the scaling of the entrance length in such a configuration. Figure 13 shows the centerline velocity and pressure profiles at peak expulsion and ingestion phases for two different Reynolds numbers (S = 10). The centerline peaks in the vena-contracta due to fluid acceleration and drops linearly in the downstream region during the expulsion phase. As shown in Fig. 13(a), the local peak increases with increasing Reynolds number. During the peak ingestion phase at Re= 50, the velocity increases right after the fluid enters the channel, while the Re = 250 case shows a sudden drop before a subsequent increase to a local maximum. Fig. 13(b) shows a nonlinear change in the centerline pressure due to the velocity gradients along the channel. This is different from the observations made by Sadri and Floryan[34] for steady flows, where it was observed that, for Re < 137, the flow does not separate and the pressure decreases linearly. Thus further simulations need to be performed in order to better assess the characteristics of the flow in this configuration.

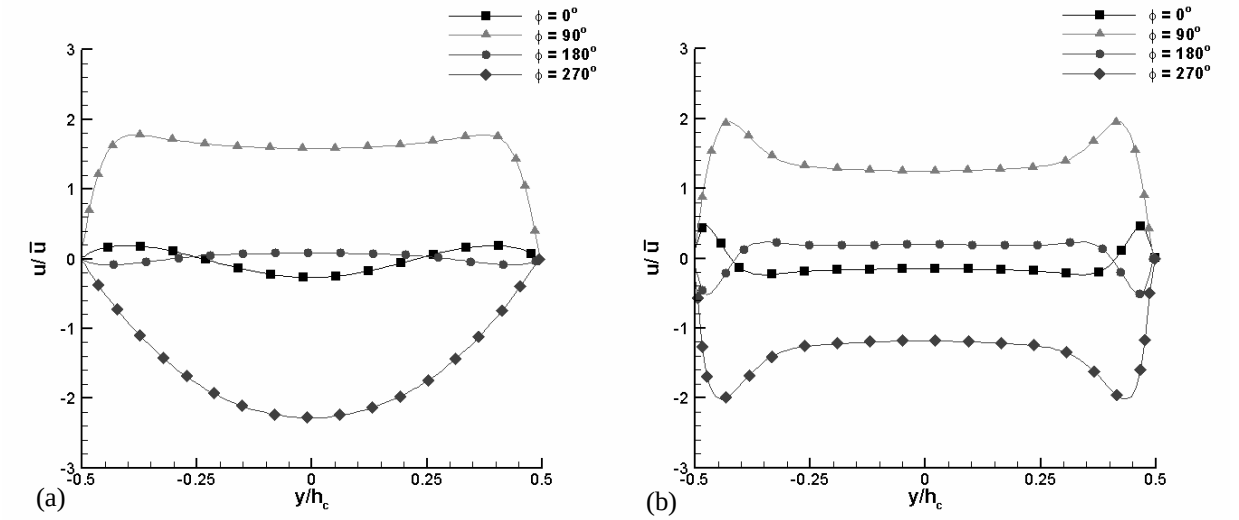

Figure 12: Velocity profiles at the entrance of a slot with a sharp entrance at Re = 100, (a) S = 5, and (b) S =30.

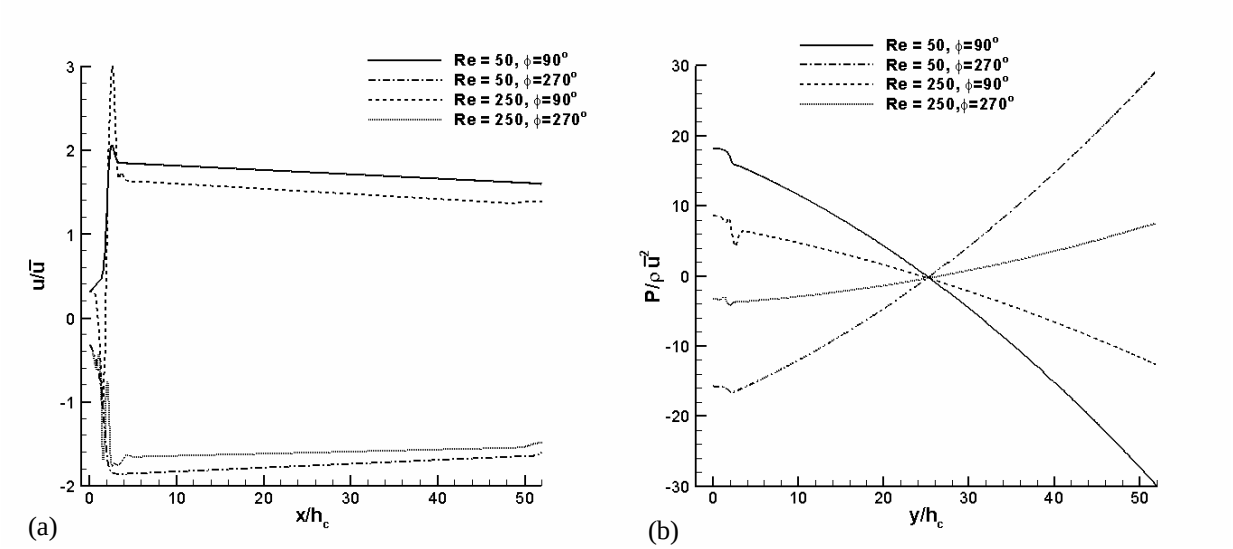

Figure 13: Centerline profiles at Re = 50 and Re = 250 for (a) velocity and (b) pressure.

V. Conclusions

Two-dimensional simulations are used to develop a scaling law for the vorticity flux from a zero-net mass-flux device operating in a crossflow laminar boundary layer. It is observed that for a fixed geometry and for a range of parameters included in the current study, the non-dimensional vorticity flux scales with the natural logarithm of jet Reynolds number (Re_j), as an inverse power (nearly -1) with the Strouhal number (St), and linearly with the ratio of the crosstream velocity to the average jet velocity ($U_\infty / \overline{V}_j$).

Next, in order to determine the pressure loss across an orifice, a semi-analytical model is formulated for an oscillatory flow in a channel. Numerical simulations are used in order to determine the scaling of entrance length at low Reynolds numbers. At higher values of both Stokes number ($S > 30$) and Strouhal number ($St > 1$) the entrance length is not influenced by Re, and shows an inverse power-law-type behavior. Preliminary simulations of oscillatory entrance flow in a slot with a sharp inlet have also been carried out. The presence of the sharp lip leads to a more complex flow with a vena-contracta, and further simulations are needed in order to characterize the entrance effects in this configuration.

Acknowledgments

This work was supported by the Air Force Office of Scientific Research grants, FA9550-05-1-0169 and F49620-03-1-0135.

References

[1]Smith, B.L. and Glezer, A., "Vectoring and Small-Scale Motions Effected in Free Shear Flows Using Synthetic Jet Actuators," AIAA Paper 97-0213, 1997.

[2]Amitay, M., Honohan, A., Trautman, M., and Glezer, A., "Modification of the Aerodynamic Characteristics of Bluff Bodies Using Fluidic Actuators," AIAA Paper 97-2004, 1997.

[3]Glezer, A. and Amitay, M., "Synthetic Jets," *Annual Review of Fluid Mechanics*, Vol. 34, pp. 503-529, 2002.

[4]Rathnasingham, R. and Breuer, K.S., "Coupled Fluid–Structural Characteristics of Actuators for Flow Control," *AIAA Journal*, Vol. 35, No. 5,pp. 832-837, 1997.

[5]Lee, C.Y., and Goldstein, D.B., "DNS of Microjets for Turbulent Boundary Layer Control," AIAA Paper 2001-1013, 2001.

[6]Crook, A. and Wood, N.J., "Measurements and Visualizations of Synthetic Jets," AIAA Paper 2001-0145, 2001.

[7]He, Y.-Y., Cary, A.W. and Peters, D.A., "Parametric and Dynamic Modeling for Synthetic Jet Control of a Post-Stall Airfoil," AIAA Paper 2001-0733, 2001.

[8]Gallas, Q., Holman, R., Nishida, T., Carroll, B., Sheplak, M., and Cattafesta, L., "Lumped Element Modeling of Piezoelectric-Driven Synthetic Jet Actuators," *AIAA Journal*, Vol. 41, No. 2, pp. 240-247, 2003.

[9]Utturkar, Y., Holman, R., Mittal, R., Carroll, B., Sheplak, M. and Cattafesta, L., "A Jet Formation Criterion for Synthetic Jet Actuators," AIAA Paper 2003-0636, 2003.

[10]Milanovi, I.M. and Zaman, K.B.M.Q., "Synthetic jets in Crossflow," *AIAA Journal*, Vol. 43, No. 5,pp.929-940, 2005.

[11]Shuster, .M. and Smith, D.R., "A Study of the Formation and Scaling of Synthetic jets," AIAA Paper 2004-90, 2004.
[12]Kelso, R. M., Lim, T.T. and Perry, A.E., "An experimental study of round jets in cross-flow," *Journal of Fluid Mechanics*, Vol. 306, pp. 83-122, 1998.
[13]Johari, H., Pacheco-Tugas, M. and Hermanson, J.C., "Penetration and mixing of pulsed jets in cross-flow," *AIAA Journal*., vol. 37, no.7, pp. 842-850, 1999.
[14]Amitay, M., Kibens, V., Parekh, D., and Glezer, A., "The Dynamics of Flow Reattachment Over a Thick Airfoil Controlled by Synthetic Jet Actuators," AIAA Paper 99-1001, 1999.
[15]Seifert, A. and Pack, L.G., "Oscillatory Control of Separation at High Reynolds Numbers," *AIAA Journal*, Vol. 37, No. 9, pp. 1062-1071,1999.
[16]Gallas, Q., Holman, R., Raju, R., Mittal, R, Sheplak, M., and Cattafesta, L., "Low Dimensional Modeling of Zero-Net Mass-Flux Actuators," AIAA Paper 2004-2413, 2004.
[17]Mittal, R and Rampunggoon, R., "On the virtual aero shaping effect of synthetic jets," *Brief Communications, Physics of Fluids*, Vol. 14, No. 4, pp. 1533-1536, 2002.
[18]Yehoshua, T. and Seifert, A. "Boundary Condition Effects on Oscillatory Momentum Generator," AIAA Paper 2003-3710, 2003.
[19]Sparrow, E.M. and Lin, S.H., "Flow Development in the Hydrodynamics Entrance Region of Tubes and Ducts," *Physics of Fluids*, Vol. 7, pp.338-347, 1964.
[20]Van Dyke, M., "Entry flow in a Channel," *Journal of Fluid Mechanics*, Vol. 44, pp. 813-823, 1970.
[21]Fargie, D. and Martin, B.W., "Developing laminar flow in a pipe of circular cross-section," *Proceedings of the Royal Society of London, Series A, Mathematical and Physical Sciences*, Vol. 321 (1546) ,pp. 461-476, 1971.
[22]Chen, R.Y., "Flow in the Entrance Region at Low Reynolds Numbers," *ASME Journal Fluids Engineering*, Vol. 95, p. 153-158, 1973.
[23]Narang, B.S., and Krishnamoorthy, G., "Laminar Flow in the Entrance Region of Parallel Plates," *ASME Journal of Applied Mechanics*, Vol. 43, pp. 186-188, 1976.
[24]Atabek, B.H and Chang, C.C., "Oscillatory flow near the entry of a circular tube," *Z.f.angew.Math & Phys.*, Vol. 12, pp.185, 1961.
[25]He, X. and Ku, D.N., "Unsteady entrance flow development in a straight tube," *Journal of Biomechanical Engineering*, Vol. 116, No.3, pp. 355-360, 1994.
[26]Kassianides, E. and Gerrad, J.H., "Calculation of Entrance length in Physiological flow," *Medical and Biological Engineering*, Vol. 13, No. 4, pp. 558-560, 1975.
[27]Goldberg, I.S. and Folk, R.T., , "Solutions for Steady and Nonsteady Entrance Flow in a semi-infinite circular tube at very Low Reynolds number," *ASME Journal of Applied Mathematics*, Vol. 48, pp. 770-791, 1988.
[28]Loudon, C. and Tordesillas, A. "The use of the dimensionless Womersley number to characterize the unsteady nature of internal flow," *Journal of Theoretical Biology*, Vol.191, pp. 63-78, 1998.
[29]Fung, Y. C. , *Biomechanics circulation*, 2nd edition, Springer-Velag, New York, pp. 188-189, 1997.
[30]Zang, Y., Street, R. L., and Kossef, J. R., "A non-staggered Grid, Fractional Step Method for Time-Dependent Incompressible Navier-Stokes Equations in Curvilinear Coordinates," *Journal of Computational Physics*, Vol. 114, pp. 18-33, 1994.
[31]Ye, T., Mittal, R., Udaykumar, H. S., and Shyy, W., "An Accurate Cartesian Grid Method for Viscous Incompressible Flows with Complex Immersed Boundaries," *Journal of Computational Physics*, Vol. 156, 1999, pp. 209-240.
[32]Najjar, F.M., and Mittal, R., "Simulations of Complex Flows and Fluid-Structure Interaction Problems on Fixed Cartesian Grids," *FEDSM 2003-45577, Proceedings of FEDSM'03*, 4th ASME-JSME Joint Fluids Engineering Conference, July 6-11, Honolulu, Hawaii, 2003.
[33]Bozkurttas, M., Dong, H., Seshadri, V., Mittal, R., Najjar, F. "Towards Numerical Simulation of Flapping Foils on Fixed Cartesian Grids," AIAA Paper 2005-0079, 2005.
[34]Sadri, R.M. and Floryan, J.M., "Accurate evaluation of the Loss coefficient and the Entrance length of the inlet region of a channel," *Journal of Fluids Engineering*, Vol. 124, pp. 685-693.
[35]Gallas, Q., "On Modeling and Design of Zero-Net Mass Flux Actuators," PhD Dissertation, Mechanical and Aerospace Engineering Department, University of Florida, Gainesville, FL, 2005.